DOI https: //doi. org/10.1007/s11595-018-1794-z

Effect of Magnesium on the C-S-H Nanostructure Evolution and Aluminate Phases Transition in Cement-Slag Blend

DING Qingjun[1], YANG Jun[1], ZHANG Gaozhan[2*], HOU Dongshuai[3]

(1. School of Materials Science and Engineering, Wuhan University of Technology, Wuhan 430070, China; 2. Advanced Building Materials Key Laboratory of Anhui Province, Anhui Jianzhu University, Hefei 230601, China; 3. Department of Civil Engineering, Qingdao Technological University, Qingdao 266033 ,China)

Abstract: The microstructural study was conducted on cement and cement-slag pastes immersed in different concentrations of $Mg(NO_3)_2$ solutions utilizing ^{29}Si, ^{27}Al NMR spectroscopy and XRD techniques. The results show that the hydration of both the cement and cement-slag pastes is delayed when the pastes are cured in $Mg(NO_3)_2$ solutions as compared to the pastes cured in water. Moreover, Mg^{2+} ions also exhibit an decalcifying and dealuminizing effect on the C-A-S-H in cement and cement-slag pastes, and thereby decrease Ca/Si and Al[4]/Si ratios of the C-A-S-H. The dealuminization of C-A-S-H is mitigated for cement-slag paste as compared to pure cement paste. The depolymerized calcium and aluminum ions from C-A-S-H gel mainly enter the pore solution to maintain the pH value and form $Al^{[6]}$ in TAH, respectively. On the other hand, Mg^{2+} ions exert an impact on the intra-transition between $Al^{[6]}$ species, from AFm and hydrogarnet to hydrotalcite-like phase. NO_3^- ions are interstratified in the layered Mg-Al structure and formed nitrated hydrotalcite-like phase ($Mg_{1-x}Al_x(OH)_2(NO_3)_x \cdot nH_2O$). Results from both ^{27}Al NMR and XRD data show that ettringite seems not to react with Mg^{2+} ions.

Key words: ^{29}Si and ^{27}Al NMR; magnesium ion; C-A-S-H microstructure; aluminate phases transition; hydration; slag incorporation

1 Introduction

With the human exploration of the ocean, more and more concrete constructions are built to serve in marine environment. However, some ions in the ocean will cause the degradation of the concrete by involving a chemical reaction of these ions with cement paste. Mg^{2+} is one of these common ions in seawater which has a deleterious effect on the concrete. Due to the limited solubility of magnesium hydroxide (brucite), it is easy to precipitate in high pH environments as often found for hydrated Portland cement paste. The depletion of hydroxyl ions will result in the leaching of calcium and destabilization of the cement hydrates. Hence, Mg^{2+} ions have always been used as the cations in testing solution during the cement exposure experiments.

Bonen[1,2] has studied the effect of magnesium sulfate on Portland cement pastes, and the results show that the samples immersed in magnesium sulfate solution produced a "transition layer" on their suface, which contained an outer magnesium hydroxide layer (about 40-120 μm in thickness) and an inner gypsum layer (about 20-70 μm in thickness). Longer time of immersion caused the formation of magnesium silicate hydrate (M-S-H) in the samples instead of calcium silicate hydrate (C-S-H). Taylor[3] studied the composition variation of C-S-H gel in plain and slag blended cement paste subject to sodium and magnesium solution and concluded that magnesium presence causes more severe decalcification of the C-S-H gel for the exposed pastes. Kunther[4] also found that $MgSO_4$ solution has an stronger decalcifying effect on synthesized C-S-H than Na_2SO_4 solution with the same sulfate concentration, even than Na_2SO_4 solution with a tenfold increase in the sulfate concentration. The above investigations have demonstrated the enhancing effect of Mg^{2+} on sulfate attack on cement paste.

On the other hand, modern cementitious pastes are often prepared with a certain level of alumina-rich supplementary cementitious materials (SCMs) replacement, which leads to an increasing amount of

(Received: Dec. 23, 2016; Accepted: Oct. 14, 2017)

DING Qingjun(丁庆军): Ph D; Prof.; E-mail: dingqj@whut.edu.cn

*Correspondent author: ZHANG Gaozhan(张高展): Ph D; Assoc. Prof.; E-mail: gaozhanzhang@126.com

Funded by National Natural Science Foundation of China (Nos. 51778513, 51402003, 51578004) and China Ministry of Science and Technology (No. 2015CB655101)

aluminum substituting into C-S-H gel[5,6], *i e*, calcium aluminosilicate hydrate (C-A-S-H) gel. Researches from experiment and molecular dynamics simulation suggest that the incorporation of aluminum in C-S-H can improve its nanomechanical properties[7,8] and seawater corrosion resistance[9,10]. As C-A-S-H gel is the main hydration product in cement paste providing cohesion strength, the Al substituting amount and coordination distribution in C-A-S-H gel are also important microstructural parameters which determine the performance and long-term durability of the pastes. As found in Ding Qingjun's research[11,12], pure cement pastes exposed to both Na_2SO_4 and $MgSO_4$ solutions exhibit a transformation from $Al^{[4]}$ in C-A-S-H and $Al^{[6]}$ in AFm to $Al^{[6]}$ in AFt.

As almost all previously reported works relevant with the magnesium ions attack on cement are performed by utilizing magnesium sulfate solutions, *i e*, the combined attack of magnesium and sulfate ions, the effect of magnesium on cement pastes is hitherto not fully understood. Therefore, $Mg(NO_3)_2$ (aq) is selected as the exposure solution in this work. Pure cement and cement pastes blended with 30 wt% granulated blast furnace slag were prepared and exposed to different concentrations (0.0%, 2.5%, 5.0% and 10.0%) of $Mg(NO_3)_2$ solutions for 28 and 365 d. After the exposure, the samples were tested by ^{29}Si, ^{27}Al NMR, SEM-EDX and XRD to investigate the hydration and the microstructure evolution in the pastes.

2 Experimental

2.1 Materials

The Portland cement(PC) and granulated blast furnace slag (GBFS) used in this experiment were P.I 52.5 cement produced by Huangshi Huaxin cement Co. LTD, China and GBFS produced by Jiangnan Grinding Co. LTD, China, respectively. The PC and GBFS used had a specific surface area of 374 m^2/kg and 454 m^2/kg, respectively, with their chemical compositions given in Table 1.

2.2 Sample preparation

Samples were prepared with water to cement ratio of 0.35 using cement containing 0% and 30 wt% slag, respectively. After 24 h of standard curing, the samples were immersed in plastic-sealed box which contained 0.0% (also denoted as water), 2.5%, 5.0% and 10.0% $Mg(NO_3)_2$ (aq) solutions, in the standard curing room. Owing to that the MgO contents were lower than 10 wt% for both materials (Table 1), and that the Mg-bearing phases (mainly being hydrotalcite) were below the detection limit of XRD for cement-slag pastes (GBFS replacement <35% by weight of binder)[5,12,13], the influence of Mg impurity in raw materials can be negligible, as compared with external Mg ions. The immersion solutions were refreshed monthly. Then samples were removed after 28 and 365 d of immersion, the outside layer of about 2 mm thickness was cut off, cracked to particles of the size of about 3 mm, and quickly treated with absolute ethanol to stop the hydration process. Finally, they were ground to fine powders and stored in a vacuum dryer at 30 ℃ for 2 h. The acquired fine powders were then sealed and stored in drying vessel for subsequent tests.

2.3 ^{29}Si and ^{27}Al NMR

The solid-state ^{29}Si and ^{27}Al magic angle spinning nuclear magnetic resonance (^{29}Si and ^{27}Al MAS NMR) spectroscopy was performed on Bruker Avance III 400 MHz spectrometers (magnetic field 9.4 T; larmor frequency of 79.5 MHz for ^{29}Si, 104.3 MHz for ^{27}Al) using magic angle spinning (MAS) chemagnetics probes with 7 and 4 mm o.d. zirconia rotors for ^{29}Si and ^{27}Al, respectively. The NMR experiments used a pulse width of 1 μs, pulse delay of 5 s, spinning speed of about 6 kHz and 2 048 scans for ^{29}Si, and a pulse delay of 1s, spinning speed of about 12 kHz and 2 048 scans for ^{27}Al. Chemical shifts for ^{29}Si were referenced with respect to the downfield resonance of tetrakis(trimethylsilyl)silane (TTMS) at -9.8 ppm, for ^{27}Al they were referenced with respect to $Al(NO_3)_3{\cdot}9H_2O$ at 0 ppm. The spectra were fitted using the Peakfit software with the line shape of Lorentz distribution, detailed method are described in Ref.[14].

2.4 SEM-EDS and X-ray diffraction

The microstructure of fractured surface samples was examined using a Japanese Hitachi SU8020 scanning electron microscope energy dispersive spectrometer (SEM-EDS), with 20 kV acceleration voltage.

Table 1 Chemical compositions of Portland cement and granulated blast furnace slag/wt%

Composition	SiO_2	Al_2O_3	Fe_2O_3	CaO	MgO	SO_3	Na_2O	K_2O	LOI
PC	21.35	4.67	3.31	62.60	3.08	2.25	0.21	0.54	0.95
GFBS	28.15	16.00	1.10	34.54	6.00	0.32	0.46	0.45	2.88

LOI: loss of ignition

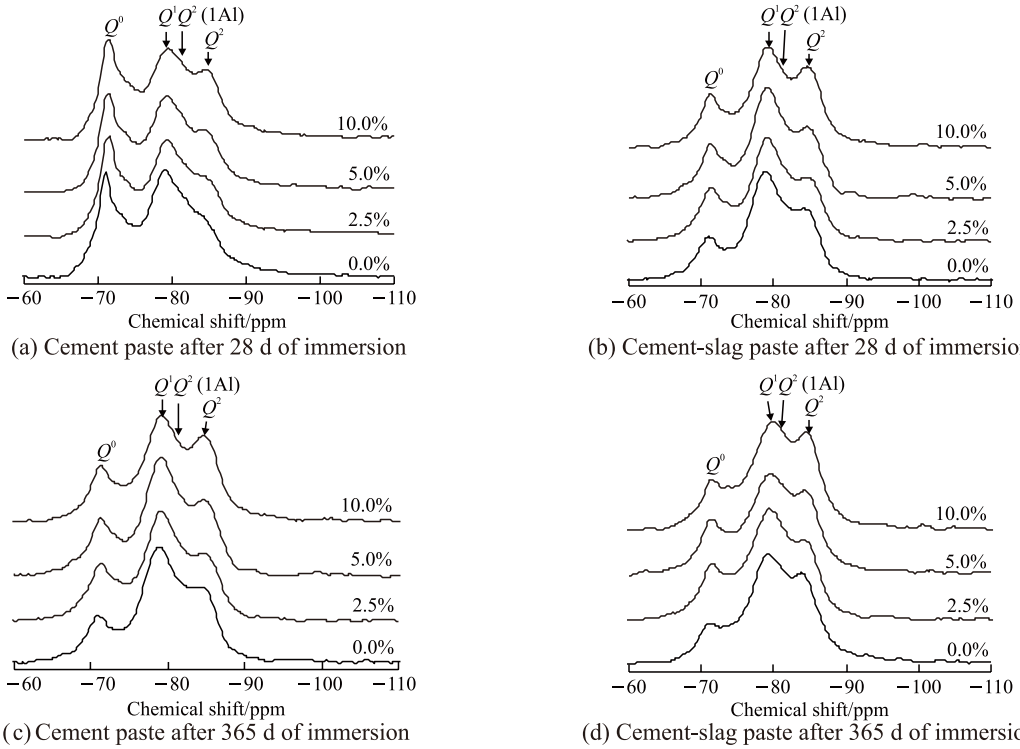

(a) Cement paste after 28 d of immersion (b) Cement-slag paste after 28 d of immersion

(c) Cement paste after 365 d of immersion (d) Cement-slag paste after 365 d of immersion

Fig.1 ^{29}Si NMR spectra for cement and cement-slag pastes immersed in different concentration of $Mg(NO_3)_2$ solutions

Bruker D8 ADVANCE X-ray diffraction analyzer was used to exam the powder of the samples. The analyses were acquired with 2θ range from 7 to 65° with a step size of 0.02° using Cu(Kα) ray in 100 mA and 40 kV.

3 Results and discussion

3.1 ^{29}Si NMR

The ^{29}Si NMR spectra of cement and cement-slag pastes exposed to water and $Mg(NO_3)_2$ solutions for 28 and 365 d are given in Fig.1. The spectra show clearly three partly overlapping resonances at -71, -79 and -85 ppm, originating from silicate tetrahedra in anhydrous minerals (Q^0), in terminal groups (Q^1) and middle groups (Q^2) of aluminosilicate chains for C-A-S-H, respectively. In addition, there also exists a resonance centered at -81.5 ppm by reference[15], which is ascribed to silicate tetrahedra connected to the substituting aluminum in the bridging sites in the aluminosilicate chains (Q^2(1Al)). A schematic diagram describing the local structure of Qn species in C-A-S-H is depicted in Fig.2. The variation in the intensities of different silicate species has been determined from deconvolution of these spectra with the results listed in Table 2. The hydration degrees of the blends and microstructural characteristics of C-A-S-H gel in the pastes, were calculated according to the following equations proposed by I. G. Richardson[16,17].

Hydration degrees of the pastes:

$$\partial = 1 - \frac{Q^0}{Q_0^0} \tag{1}$$

Mean Chain length of C-A-S-H gel:

$$MCL = \frac{Q^1 + Q^2 + 1.5Q^2(1A1)}{0.5Q^1} \tag{2}$$

Al[4] to Si ratios of C-A-S-H gel:

$$Al[4]/Si = \frac{0.5Q^2(1A1)}{Q^1 + Q^2 + Q^2(1A1)} \tag{3}$$

3.1.1 Hydration degrees

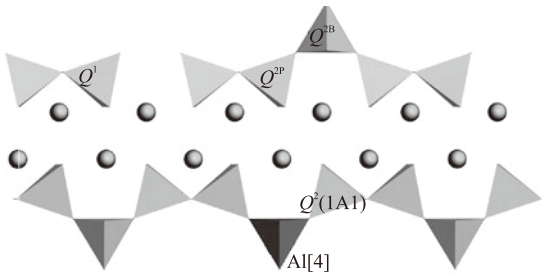

Fig.2 Schematic diagram of silicate tetrahedra species in C-A-S-H

The hydration degrees of cement and cement-slag pastes immersed in different type of solutions for 28 and 365 d are depicted in Fig.3 as column diagram. It can be noted that the hydration degree of water exposure cement paste increases with hydration age, which are 72.92% and 85.03% for 28 and 365 d hydration

Table 2 Deconvolution results of ^{29}Si NMR spectra for cement and cement-slag pastes under the attack of magnesium ions

Slag content/%	Mg^{2+} ions concentration/%	Age/d	Relative intensities of Q^n species/%				
			Q^0	Q^1	Q^2(1Al)	Q^{2B}	Q^{2P}
0.0	0.0	28	27.99	49.88	7.25	5.01	9.87
	2.5		34.74	36.80	5.46	7.68	15.32
	5.0		35.11	34.80	4.89	8.57	16.63
	10.0		36.66	31.25	3.47	9.51	19.11
30.0	0.0		35.01	37.18	8.47	6.48	12.86
	2.5		37.36	31.97	8.07	7.87	14.73
	5.0		39.03	30.07	7.56	8.08	15.26
	10.0		41.19	25.78	7.72	8.62	16.68
0.0	0.0	365	15.31	53.21	4.24	9.13	18.10
	2.5		19.21	42.48	3.33	11.74	23.23
	5.0		20.22	40.60	2.14	12.41	24.62
	10.0		21.46	35.50	2.03	13.62	27.38
30.0	0.0		16.21	41.02	10.99	10.78	21.00
	2.5		18.16	37.92	10.05	11.35	22.53
	5.0		18.80	34.03	8.87	13.17	25.13
	10.0		20.24	30.90	7.92	13.56	27.38

of the paste, respectively. The hydration degrees are 66.88% and 84.17% for cement-slag after 28 and 365 d of immersion in water. Zhiliang Wang[18] have studied the hydration degree of cement paste by different test methods, and the results show that 28 d hydration degrees of cement paste were 73.32%, 77.14% and 73.17% for chemical bond water and hydration heat flow method, respectively. The hydration degrees of the pastes calculated by Q^n species proportion in ^{29}Si NMR spectra in this paper are in good agreement with Yuxue Zhu's research, which shows the capability of NMR in the characterization of cement hydration.

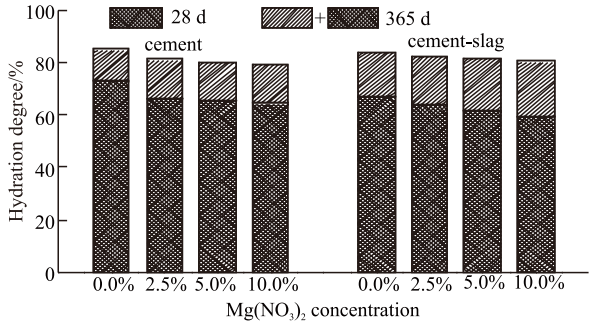

Fig.3 Hydration degrees of cement and cement-slag pastes after 28 and 365 days of immersion in $Mg(NO_3)_2$ solutions

The 28 d hydration degree of cement-slag paste is lower than that of cement paste, while 365 d hydration degrees of cement and cement-slag pastes are similar. The lower reaction degree of cement-slag paste at hydration age of 28 d as compared to cement paste is due to the lower hydration reactivity of supplementary cementitious material – slag. At hydration age of 365 d, the hydration degree of slag can reach about 75% due to pozzolanic reaction[19], which is close to that of pure cement, leading to the increasing hydration degree of cement-slag paste.

Hydration degrees of the pastes decrease to various extents, when samples are immersed in different concentrations of $Mg(NO_3)_2$ solutions. Hydration degrees decrease by 3.8% and 1.9% for cement and cement-slag pastes, respectively, after 365 d exposure to 2.5% $Mg(NO_3)_2$ solution as compared to paste exposure to water, 5.0% and 2.3% when exposure to 5.0% $Mg(NO_3)_2$ solution. This is due to the $Mg(OH)_2$ precipitation around the samples which inhibit the transportation of water and ions, thus delaying the hydration of the paste.

3.1.2 Mean chain lengths of C-A-S-H gel

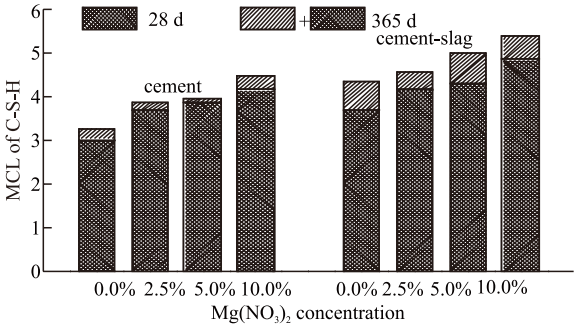

Fig.4 MCLs of C-A-S-H gel in cement and cement-slag pastes after 28 and 365 days of immersion in $Mg(NO_3)_2$ solutions

The MCLs of C-A-S-H in cement and cement-slag pastes immersed in different type of solutions for 28 and 365 d are illustrated in Fig.4. The MCLs of C-A-S-H for water exposure cement and cement-slag paste increase with age, implying the polymerization of sili-

cate tetrahedra as hydration progresses. MCLs of C-A-S-H gel are 3.03 and 3.26 for cement paste after 28 and 365 d of water-curing, respectively, which is consistent with Rodger's result[20]. It can be observed that the incorporation of slag leads to longer silicate chains formation in C-A-S-H phases, which is associated with a reducing molar Ca/Si ratio of the cement-slag paste and thus a lower Ca/Si ratio for C-A-S-H phases. As is described in[21], the polymerization degree of silicate tetrahedra increases, thus increasing MCL with the decrease of Ca/Si ratio of C-A-S-H gel.

When the samples are immersed in $Mg(NO_3)_2$ solutions, the MCLs of C-A-S-H gel in both cement and cement-slag pastes increase, and this increment in MCL extends with increasing concentration of $Mg(NO_3)_2$, which can be explained by the decalcifying effect of Mg^{2+} ions on C-A-S-H gel. Mg^{2+} ingress into the samples can react with OH^- to form $Mg(OH)_2$, which has a lower solubility and tends to precipitate, hence the pH value in the pore solution of the sample decreases. C-A-S-H gels in acidic or neutral pH environments tend to release Ca^{2+} and transform into lower Ca/Si C-A-S-H gel with longer silicate chains.

3.1.3 Al[4]/Si ratios of C-A-S-H gel

The Al[4]/Si ratios of C-A-S-H in cement and cement-slag pastes immersed in different concentrations of $Mg(NO_3)_2$ solutions for 28 d and 365 d are illustrated in Fig.5. The Al[4]/Si ratios of C-A-S-H decrease with hydration age for water-curing cement sample, reflecting the gradual migration of substituted aluminum from silicate chains. This could be ascribed to the longer Al-O bond as compared to Si-O bond, which leads to the aluminum substitution in tetrahedral sites of the silicate chains being thermodynamically unstable. This phenomenon is consistent with the progressive richer in silicon for C-A-S-H gel observed by Fernández-Jimenez in alkali-activated fly ash pastes[22,23]. In the case of slag blended sample, it has a higher Al[4]/Si ratio for C-A-S-H gel and the ratio is slightly increases from hydration age of 28 to 365 d. This increase may involve the pozzolanic reaction of slag, which mainly occurs after 28 d of cement hydration and releases Al^{3+} ions available for substitution in C-A-S-H gel, thus improving the Al[4]/Si ratio of C-A-S-H gel.

The Al[4]/Si ratios of C-A-S-H gel are lower for both cement and cement-slag pastes when the samples are immersed in $Mg(NO_3)_2$ solutions, and the decreases in Al[4]/Si ratios are more evident as the $Mg(NO_3)_2$ concentration increases. This my reflect that Mg^{2+} ions exhibit a dealuminizing effect on C-A-S-H gel. The decrements of Al[4]/Si ratio in C-A-S-H gel are minor for slag blended samples, indicating that the blend of slag can improve the structural stability of C-A-S-H when it is subjected to magnesium attack.

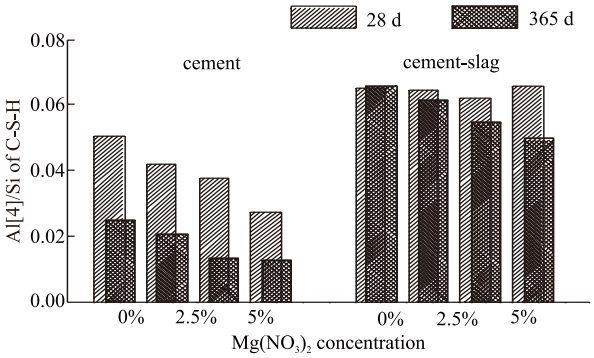

Fig.5 Al[4]/Si ratios of C-A-S-H gel in cement and cement-slag pastes after 28 and 365 days of immersion in $Mg(NO_3)_2$ solutions

3.2 SEM-EDS

In order to understand the relationship between the MCL and composition of C-A-S-H phases thoroughly, SEM-EDS analyses of C-A-S-H gel in part of the samples were performed (cement and cement-slag paste exposed to water, cement-slag paste exposed to 5% $Mg(NO_3)_2$ solution). Fig.6 is the representative chemical composition of C-A-S-H gel in pastes. The EDS analyses suggest strong peaks of Ca, Si Al and O for all the samples, indicating the presence of cal-

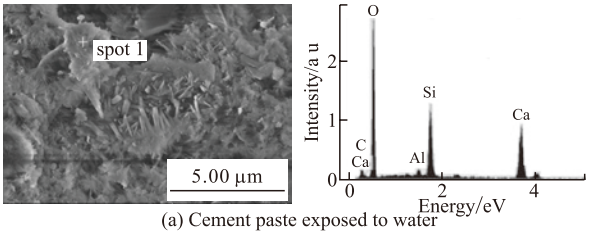

(a) Cement paste exposed to water

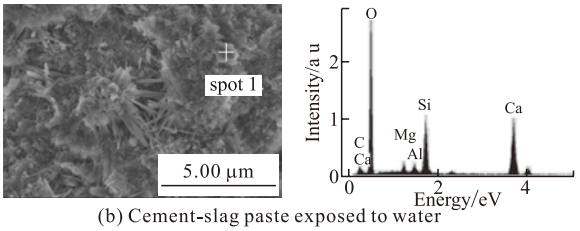

(b) Cement-slag paste exposed to water

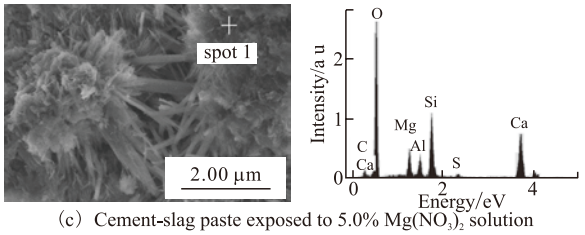

(c) Cement-slag paste exposed to 5.0% $Mg(NO_3)_2$ solution

Fig.6 SEM-EDS analyses of cement and cement-slag pastes after 365 days of exposure to different solutions

cium aluminosilicate hydrates. The presence of peaks assigned to carbon element suggests that the C-A-S-H phases are slightly carbonated, which may occur during the preparation of the sample. Twenty points was analyzed for each of these samples and the Ca/Si ratio distribution of C-A-S-H is plotted in Fig.7 as scattering diagram.

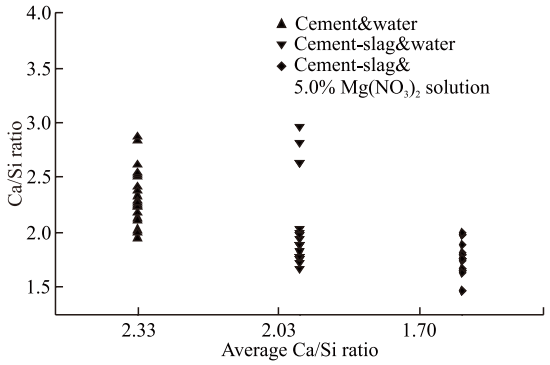

Fig.7 Ca/Si ratio distribution of C-A-S-H gel in the selected samples after 365 days of exposure to different solutions

The average Ca/Si ratio of C-A-S-H in cement paste is 2.33 (See Fig.7), which is a little higher than those in other researchers' work. The excess in Ca/Si ratio of C-A-S-H phase can be explained by the intermixture of C-A-S-H with portlandite at the scale too fine to be distinguished by energy dispersive spectroscopy probe. Both the incorporation of slag and exposure to 5% $Mg(NO_3)_2$ solutions lead to a decrease in Ca/Si ratio of C-A-S-H in the samples, which is in agreement with the NMR data, proving that lower Ca/Si C-A-S-H gel has longer silicate chains in its structure.

3.3 ^{27}Al NMR

The ^{27}Al NMR spectra of cement and cement-slag pastes exposed to water and $Mg(NO_3)_2$ solutions for 28 and 365 d are given in Fig.8. Peaks at 74 and 60 ppm can be assigned to tetra-coordinated Al (Al[4]) in C-A-S-H[24] and anhydrous slag (Fig.8(c)). Aluminum in AFt, AFm and Third Aluminate Hydrate (TAH) are hexa-coordinated (Al[6]), which shows resonances at 13.2, 10.0 and 4.1 ppm, respectively. TAH is an amorphous phase precipitated on the surface of C-A-S-H phase[25], which exsits in the form of $[Al(OH)_6]^{3-}$ or $[O_xAl(OH)_{6-x}]^{(3+x)-}$. For slag blended pastes, there also shows a slightly raised peak centered at about 34 ppm belonging to penta-coordinated aluminum (Al[5])[26]. In addition, there exists a resonance with chemical shift ≈ 9.0 ppm designated to hydrotalcite-like phase (*i e*, a Mg-Al layered double hydroxide (Mg-Al LDH)) in the spectra for pastes with slag addition and high MgO content[27,28]. Peaks of hydrotalcite-like and AFm phases

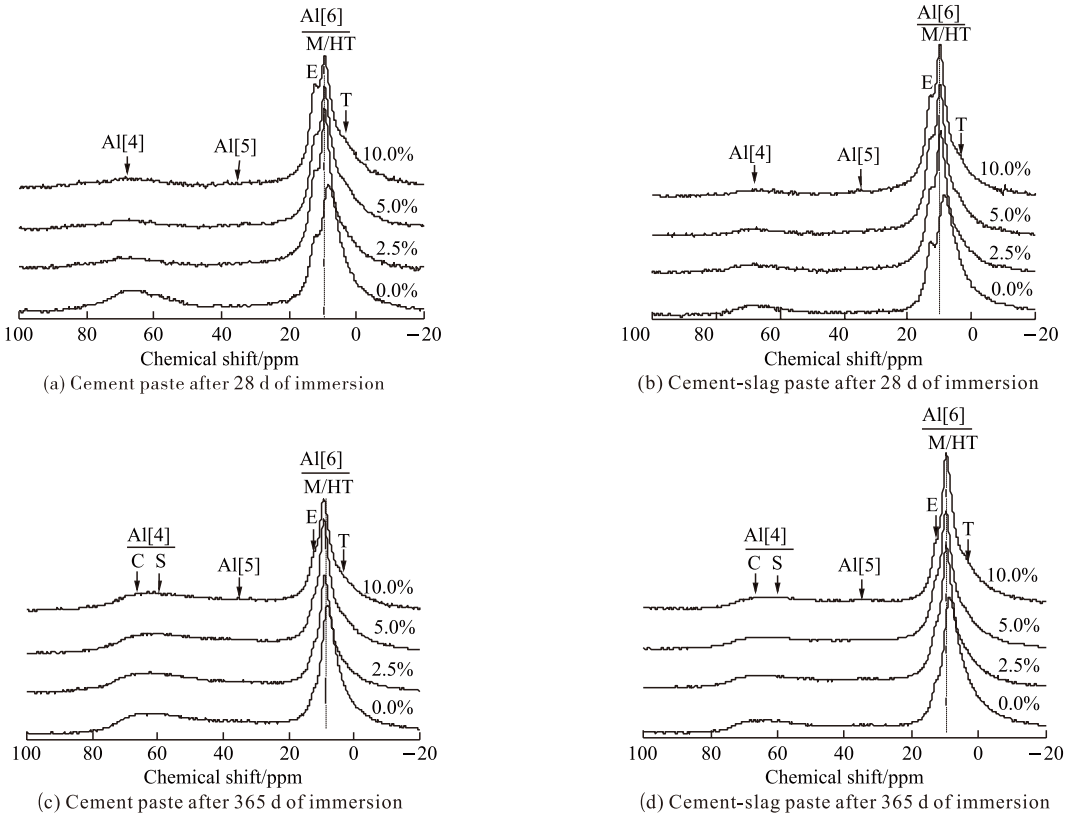

Fig.8 ^{27}Al NMR spectra for cement and cement-slag pastes immersed in different concentration of $Mg(NO_3)_2$ solutions (T-Al[6] in TAH; M/HT-Al[6] in AFm or hydrotalcite-like; E-Al[6] in AFt; S-Al[4] in slag; C-Al[4] in the C-A-S-H)

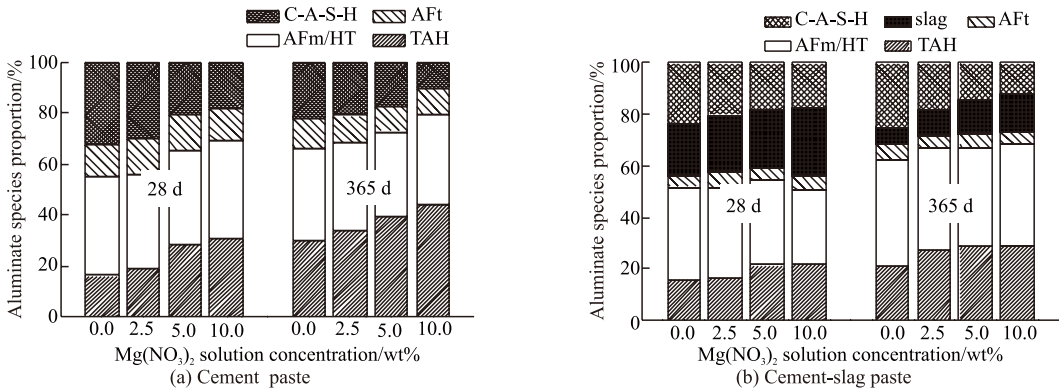

Fig.9 Aluminate species proportion in cement and cement-slag pastes after 28 and 365 days of immersion in $Mg(NO_3)_2$ solutions

can't be differentiated clearly in the spectra due to the similar chemical shifts of these two phases. Nevertheless, the slight shift in position to upfield and decrease in full width at half maximum (FWHM) of the overlapping resonances for these two phases can demonstrate the phase transition occurring from AFm in water-curing samples to hydrotalcite-like phase in $Mg(NO_3)_2$ solutions curing samples.

To quantitatively study the aluminate species transition in the samples, deconvolution of the spectra was performed. As aluminum in cement clinker mainly exists in C_3A mineral which is almost fully hydrated after 3 days, the contribution from anhydrous cement in the spectra is not considered in the fitting process. Hydrotalcite-like and AFm phases are taken as a mixture (M/HT) phase, for their resonances overlap with each other. The deconvolution results of these spectra are plotted as stack column in Fig.9.

With increasing hydration age and $Mg(NO_3)_2$ concentration, the relative proportion of aluminum in C-A-S-H decreases (See Fig.9), which is in accordance with the fitting results of ^{29}Si NMR spectra. The relative proportion of aluminum in C-A-S-H is higher for slag blended paste than for pure cement paste, indicating more aluminum entering the bridging position of silicate chains of C-A-S-H. Moreover, it can be observed from Fig.9(b) that the amount of anhydrous slag in the paste increases with increasing concentration of $Mg(NO_3)_2$. This is in agreement with the results in Section 3.1.1, proving that Mg^{2+} ions' presence can delay the hydration of cement-slag paste.

For water-curing cement paste, the amount of AFt decreases and AFm increases from 28 to 365 d (Fig.9(a)), implying the gradual transformation from AFt to AFm. The amount of Al in C-A-S-H is lower for cement sample cured with increasing concentration of $Mg(NO_3)_2$ solution, which suggests that Mg^{2+} ions have a dealuminizing effect on C-A-S-H. This part of aluminum may turn into TAH phase, as shown in Fig.9(a) that TAH becomes more prominent with increasing $Mg(NO_3)_2$ concentration. When the samples are blended with slag, the proportion of each phase changes (Fig.9(b)). Firstly, the AFt content in the samples obviously decreases as compared to pure cement samples, which is typical for aluminum-rich pastes. Secondly, cement-slag pastes display a larger increment in AFm/HT content and a minimal decrement in Al in C-A-S-H content from hydration age of 28 to 365 d. This can be explained by the hydration of slag, which provides enough Al^{3+} to form C-A-S-H and AFm/HT. Lastly, the amount of AFt appears to be independent of $Mg(NO_3)_2$ concentrations for both cement and cement-slag samples, reflecting that this phase don't react with Mg^{2+} ions.

3.4 X-ray diffraction

X-ray diffraction was also employed to study the phase transition of cement-slag paste after 365 d of immersion in $Mg(NO_3)_2$ solutions of the concentration of 0.0%, 2.5% and 10.0% by weight with the diffractograms shown in Fig. 10. The patterns show that the diffraction intensity of portlandite decreases and brucite increases for samples cured in more concentrated $Mg(NO_3)_2$ solution, which suggests a large number of brucite production at the expense of portlandite. This also accounts for the decrease in pH value of the pore solutions when Mg^{2+} ions are present. Weak peaks of hemicarbonate are observed for water-curing cement-slag paste, implying slight carbonation of the sample. Moreover, peaks at 2θ = 10.2° and 20.5° are observed in the patterns for samples immersed in $Mg(NO_3)_2$ solutions, indicating the transformation from AFm to hydrotalcite-like phase. This phase was also detected in MgO modified alkali-activated slag paste[5] [28], where the peaks from hydrotalcite-like phase at 2θ = 11.7° and 23.4° are clearly observed. The shift of the reflection for hydrotalcite-like phase to lower 2θ an-

gles in this work has been related to the NO_3^- presence which is interstratified in the layered Mg-Al structure, $Mg_{1-x}Al_x(OH)_2(NO_3)_x \cdot nH_2O$, where x = 0.20-0.34[29]. For samples cured in $Mg(NO_3)_2$ solutions, peaks for carbonate phases were not detected above the noise level, implying the instability of these phases. There also exhibit small peaks of ettringite for all the tested samples. These peaks are all with similar intensities regardless of the type of curing solution, which is corresponding to the results from ^{27}Al NMR spectra.

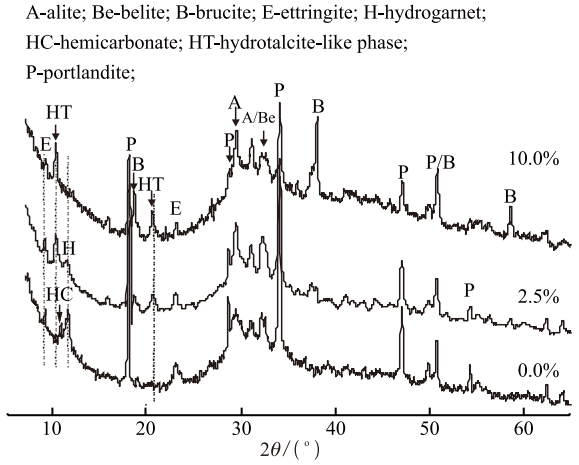

Fig.10 XRD patterns of cement-slag pastes immersed in different concentrations of $Mg(NO_3)_2$ solutions for 365 days

3.5 Microstructure evolution mechanism for cement-slag blend in the presence of Mg^{2+} ions

Through the analyses of the above experimental results, the microstructure evolution mechanism for cement-slag blend in the presence of Mg^{2+} ions can be hypothesized as follows:

Mg^{2+} ions penetrated into cement paste will first react with OH^- to form $Mg(OH)_2$, which precipitates in the outer layer[1] of the sample and thus inhibits the diffusion of water and ions. Hence, the $Mg(OH)_2$ precipitate around the sample can delay the hydration of the paste. On the other hand, the $Mg(OH)_2$ formation can lead to the decrease in pH value of the pore solution and decalcification of C-A-S-H gel. Decalcification will lead to structural regulation of the silicate tetrahedra, where longer silicate chains are formed to balance the deficit in positive charge due to the removal of interlayer calcium ions. The substituted aluminum may depolymerize from the silicate chains during the regulation process thereby resulting in decreasing Al[4]/Si ratio for C-A-S-H. This part of depolymerized aluminum mostly transforms into TAH. When the cement pastes are blended with slag, the dealuminizing effect of Mg^{2+} ions on the C-A-S-H phase is mitigated. This is because of the pozzolanic reaction of slag at later hydration age (28-365 d) which can release Al^{3+} available for the secondary formation of C-A-S-H. Furthermore, magnesium ions can also exert an impact on the intra-transition between Al[6] species, from AFm and hydrogarnet to hydrotalcite-like phase, where the released calcium ions may enter the pore solution to keep the pH value of the environment. Overall, the reaction equations can be expressed as follows:

$$Mg^{2+}+OH^- \rightarrow Mg(OH)_2 \quad (4)$$

$$\text{High Ca/SiC-S-H}+H_2O \rightarrow \text{Low Ca/SiC-S-H}+Ca^{2+}+OH^- \quad (5)$$

$$4CaO \cdot Al_2O_3 \cdot 13H_2O+Mg^{2+}+NO^-_3 \rightarrow Mg_{1-x}Al_x(OH)_2(NO_3)_x \cdot nH_2O+Ca^{2+} \quad (6)$$

$$3CaO \cdot Al_2O_3 \cdot 6H_2O+Mg^{2+}+NO^-_3 \rightarrow Mg_{1-x}Al_x(OH)_2(NO_3)_x \cdot nH_2O+Ca^{2+} \quad (7)$$

Most of the studies have reported that large amount of ettringite and gypsum were formed in pure cement or blended paste during magnesium sulfate attack, whereas no hydrotalcite-like phase was found[1]. This may suggest that hydrotalcite-like phase can only be formed when there is no excessive sulfate in the paste, high sulfate concentration would lead to the decomposition of this phase and the formation of ettringite. On the other hand, ettringite as a alkaline cement hydration product dissolves when the environmental pH is below 10.7[30]. It should be noted from the NMR and XRD data that the ettringite has been existing even after 365 d of immersion in the $Mg(NO_3)_2$ solutions, which indicates that the pH in the pore solution is still maintained at a higher value by dissolving of portlandite and decalcifying of C-A-S-H. More concentrated solutions or longer ages of immersion are needed to consume the $Ca(OH)_2$ in the pastes and then to decompose the ettringite.

4 Conclusions

This study involves the characterization of microstructure of cement and cement-slag pastes immersed in different concentrations of $Mg(NO_3)_2$ solutions. The hydration of both the cement and cement-slag pastes is delayed when the pastes is cured in $Mg(NO_3)_2$ solutions as compared to the pastes cured in water. Additionally, Mg^{2+} ions exhibit a decalcifying effect on the C-A-S-H in cement and cement-slag pastes. The decalcification

of the C-A-S-H is accompanied by a prolonged MCL of its aluminosilicate chains. Mg^{2+} ions' presence would also cause the depolymerization of aluminum substituted in the silicate chains and thus the decrease in Al[4]/Si ratio of the C-A-S-H (denoted as dealuminization) in cement and cement-slag pastes, the latter shows weak dealuminization due to pozzolanic reaction of the slag. This part of depolymerized aluminum mianly forms $Al^{[6]}$ in TAH. On the other hand, Mg^{2+} ions exert an impact on the intra-transition between $Al^{[6]}$ species, from AFm and hydrogarnet to hydrotalcite-like phase, as indicated by ^{27}Al NMR and XRD analyses. NO_3^- ions are interstratified in the layered Mg-Al structure and formed nitrated hydrotalcite-like phase ($Mg_{1-x}Al_x(OH)_2(NO_3)_x \cdot nH_2O$), causing the shift of this phase reflection in XRD diffractograms. Ettringite is detected for all the samples, whose amounts seem to be independent of the type of curing solution, meaning that this phase doesn't react with Mg^{2+} ions.

^{27}Al NMR spectroscopy is a powerful tool for the quantitative analysis of different aluminate species. However, the close chemical shifts of AFm and hydrotalcite-like phases, as well as the stronger second-order quadrupolar broadening at low magnetic field (9.4 T), results in the difficulty in distinguishing the overlapping resonances of these two phases in the spectra. Perhaps NMR spectrometer with higher magnetic field (18.8 T) can be utilized to quantitatively study the transition between these two phases in the near future.

References

[1] Bonen D, Cohen M D. Magnesium Sulfate Attack on Portland Cement Paste-I. Microstructural Analysis[J]. *Cement & Concrete Research*, 1992, 22(1): 169-180

[2] Bonen D, Cohen M D. Magnesium Sulfate Attack on Portland Cement Paste—II. Chemical and Mineralogical Analyses[J]. *Cement & Concrete Research*, 1992, 22(4): 707-718

[3] Gollop R S, Taylor H F W. Microstructural and Microanalytical Studies of Sulfate Attack. IV. Reactions of a Slag Cement Paste with Sodium and Magnesium Sulfate Solutions[J]. *Cement & Concrete Research*, 1996, 26(26): 1 013-1 028

[4] Kunther W, Lothenbach B, Skibsted J. Influence of the Ca/Si Ratio of the C–S–H Phase on the Interaction with Sulfate Ions and Its Impact on the Ettringite Crystallization Pressure[J]. *Cement & Concrete Research*, 2015, 69(1): 37-49

[5] Taylor R, Richardson I G, Brydson R. Composition and Microstructure of 20-year-old Ordinary Portland Cement-ground Granulated Blast-furnace Slag Blends Containing 0 to 100% Slag[J]. *Cement & Concrete Research*, 2010, 40(40): 971-983

[6] Dai Z, Tran T T, Skibsted J. Aluminum Incorporation in the C–S–H Phase of White Portland Cement-Metakaolin Blends Studied by ^{27}Al and ^{29}Si MAS NMR Spectroscopy[J]. *Journal of the American Ceramic Society*, 2014, 97(8): 2 662-2 671

[7] Hou D, Li Z, Zhao T. Reactive Force Field Simulation on Polymerization and Hydrolytic Reactions in Calcium Aluminate Silicate Hydrate (C-A-S-H) Gel: Structure, Dynamics and Mechanical Properties[J]. *Rsc Advances*, 2015, 5(1): 448-461

[8] Qomi M J A, Ulm F J, Pellenq J M. Evidence on the Dual Nature of Aluminum in the Calcium-Silicate-Hydrates Based on Atomistic Simulations[J]. *Journal of the American Ceramic Society*, 2012, 95(3): 1 128-1 137

[9] Jackson M D, Moon J, Gotti E, *et al.* Material and Elastic Properties of Al-Tobermorite in Ancient Roman Seawater Concrete[J]. *Journal of the American Ceramic Society*, 2013, 96(8): 2 598-2 606

[10] Jackson M D, Chae S R, Mulcahy S R, *et al.* Unlocking the Secrets of Al-tobermorite in Roman Seawater Concrete[J]. *American Mineralogist*, 2013, 98(10): 1 669-1 687

[11] Ding Q, Wang H, Hu C, *et al.* Effect of Corrosive Solutions on C-S-H Microstructure in Portland Cement Paste with Fly Ash[J]. *Journal of Wuhan University of Technology-Materials Science Edition*, 2016, 31(5): 1 002-1 007

[12] Ding Qingjun, Liu Kai, Zhang Gaozhan, *et al.* The Composition and Al-bearing Phases Transition of Cement Paste Subjected to $MgSO_4$ attack[J]. *Journal of Wuhan University of Technology*, 2016, 38(5):1-7(in Chinese)

[13] Mendes A, Gates W P, Sanjayan J G, *et al.* NMR, XRD, IR and Synchrotron NEXAFS Spectroscopic Studies of OPC and OPC/Slag Cement Paste Hydrates[J]. *Materials & Structures*, 2011, 44(10): 1 773-1 791

[14] Jakobsen H J, Hall C. Quantification of Calcium Silicate Phases in Portland Cements by ^{29}Si MAS NMR Spectroscopy[J]. *Journal of the Chemical Society Faraday Transactions*, 1995, 91(24): 4 423-4 430

[15] Brough A R, Dobson C M, Richardson I G, *et al. In Situ* Solid-State NMR Studies of Ca_3SiO_5: Hydration at Room Temperature Using ^{29}Si Enrichment[J]. *Journal of Materials Science*, 1993, 29(15): 3 926-3 940

[16] Girão A V, Richardson I G, Porteneuve C B, *et al.* Composition, Morphology and Nanostructure of C–S–H in White Portland Cement Pastes Hydrated at 55 ℃[J]. *Cement & Concrete Research*, 2007, 37(12): 1 571-1 582

[17] Richardson I G. Tobermorite/Jennite- and Tobermorite/Calcium Hydroxide-based Models for the Structure of C-S-H: Applicability to Hardened Pastes of Tricalcium Silicate, *β*-dicalcium Silicate, Portland Cement, and Blends of Portland Cement with Blast-furnace Slag, Metakaol[J]. *Cement & Concrete Research*, 2004, 34(9): 1 733-1 777

[18] Wang Zhiliang, Ding Qingjun. Comparative Study on Characterization Methods of Integrate Hydration Degree of Fly Ash and Cement Composite Blend Pastes[J]. *Journal of Wuhan University of Technology*, 2014, 36(1):17-23(in Chinese)

[19] Lumley J S, Gollop R S, Moir G K, *et al.* Degrees of Reaction of the Slag in Some Blends with Portland Cements[J]. *Cement & Concrete Research*, 1996, 26(1): 139-151

[20] Rodger S A, Groves G W, Clayden N J, *et al.* A Study of Tricalcium Silicate Hydration from Very Early to Very Late Stages[J]. *Materials Research Society Symposium Proceedings*, 1987, (85): 13-20

[21] Cong X, Kirkpatrick R J. ^{29}Si MAS NMR Study of the Structure of Calcium Silicate Hydrate[J]. *Advanced Cement Based Materials*, 1996, 3(3): 144-156

[22] Fernández-Jimenez A, Torre A G D L, Palomo A, *et al.* Quantitative Determination of Phases in the Alkali Activation of Fly Ash. Part I. Potential Ash Reactivity[J]. *Fuel*, 2005, 85(5-6): 625-634

[23] Fernández-Jiménez A, Torre A G D L, Palomo A, *et al.* Quantitative Determination of Phases in the Alkaline Activation of Fly Ash. Part II: Degree of Reaction[J]. *Fuel*, 1960, 85(14-15): 1 960-1 969

[24] Andersen M D, Jakobsen H J, Skibsted J. Incorporation of Aluminum in the Calcium Silicate Hydrate (C-S-H) of Hydrated Portland Cements: a High-field ^{27}Al and ^{29}Si MAS NMR Investigation[J]. *Inorganic Chemistry*, 2003, 42(7): 2 280-2 287

[25] Andersen M D, Jakobsen H J, Skibsted J. A New Aluminium-hydrate Species in Hydrated Portland Cements Characterized by Al and Si MAS NMR Spectroscopy[J]. *Cement & Concrete Research*, 2006, 36(1): 3-17

[26] Sun G K, Young J F, Kirkpatrick R J. The Role of Al in C–S–H: NMR, XRD, and Compositional Results for Precipitated Samples[J]. *Cement & Concrete Research*, 2006, 36(1): 18-29

[27] Le S G, Mohsen B H, Frank W, *et al.* Hydration Degree of Alkali-Activated Slags: A ^{29}Si NMR Study[J]. *Journal of the American Ceramic Society*, 2011, 94(12): 4 541-4 547

[28] Jin F, Gu K, Al-Tabbaa A. Strength and Drying Shrinkage of Reactive MgO Modified Alkali-activated Slag Paste[J]. *Construction & Building Materials*, 2014, 51(4): 395-404

[29] And Z P X, Zeng H C. Decomposition Pathways of Hydrotalcite-like Compounds $Mg_{1-x}Al_x(OH)_2(NO_3)_x \cdot nH_2O$ as a Continuous Function of Nitrate Anions[J]. *Chemistry of Materials*, 2001, 13(12): 4 564-4 572

[30] Myneni S C B, Traina S J, Logan T J. Ettringite Solubility and Geochemistry of the $Ca(OH)_2$–$Al_2(SO_4)_3$–H_2O System at 1 atm Pressure and 298 K[J]. *Chemical Geology*, 1998, 148(148): 1-19